

Generation and applications of a broad atomic oxygen beam with a high flux-density via collision-induced dissociation of O₂

Zhiqiang Han¹, Liying Song¹, Po-Wan Shum², and Woon-Ming Lau³

¹University of Science and Technology Beijing

²University of Science and Technology Beijing Shunde Innovation School

³Linyi University

April 13, 2024

Abstract

We detail the generation of a pulsed atomic oxygen (AO) broad beam with a high flux-density via collision-induced dissociation of O₂ to support practical industrial exploitation of AOs, particularly for facilitating 2-dimensional oxidation/etching at a fast rate of one-monolayer per second in an area [?]1000cm². This innovation fuses the following interdisciplinary concepts: (a) a high density of O⁺ can be produced in an electron-cyclotron-resonance (ECR) O₂ plasma; (b) O⁺ can be extracted and accelerated with an aperture-electrode in the plasma; (c) O⁺ with adequate kinetic energy can initiate a cascade of gas-phase collisions in the presence of O₂; (d) collision-induced dissociation of O₂ yields AOs with adequate kinetic energy which can cause additional collision-induced dissociation of O₂. Computational simulations of such collisions, with both ab initio molecular dynamics and direct simulation Monte Carlo methods, are used to guide the experimental generation of the proposed AO-beam. We experimentally demonstrate the highest known AO mean flux-density of about 1.5×10^{16} atoms cm⁻² s⁻¹ in a broad-beam, and use it to oxidatively modify a self-assembled molecular layer of siloxane on a silicon wafer. In addition, we also demonstrate the growth of Al₂O₃ through an AO-assisted atomic layer deposition process at a room temperature.

Generation and applications of a broad atomic oxygen beam with a high flux-density via collision-induced dissociation of O₂

Zhiqiang Han^{a,b}, Liying Song^{a,b}, Po-Wan Shum^{b,d*}, Woon-Ming Lau^{c,a,b,*}

^a Beijing Advanced Innovation Center for Materials Genome Engineering, Center for Green Innovation, School of Mathematics and Physics, University of Science and Technology Beijing, Beijing 100083, China^b Shunde Innovation School, University of Science and Technology Beijing, Foshan, Guangdong 528399, China

^c School of Chemistry and Chemical Engineering, Linyi University, Linyi, Shandong, 276000, China

^d The Sun Age (Guangdong) New Energy Ltd, China

Corresponding Author

*Woon-Ming Lau. Email: leolau@lyu.edu.cn

*Po-Wan Shum. Email: samshum@thesunage.com

Abstract

We detail the generation of a pulsed atomic oxygen (AO) broad beam with a high flux-density via collision-induced dissociation of O₂ to support practical industrial exploitation of AOs, particularly for facilitating 2-dimensional oxidation/etching at a fast rate of one-monolayer per second in an area [?]1000cm². This innovation fuses the following interdisciplinary concepts: (a) a high density of O⁺ can be produced in an

electron-cyclotron-resonance (ECR) O_2 plasma; (b) O^+ can be extracted and accelerated with an aperture-electrode in the plasma; (c) O^+ with adequate kinetic energy can initiate a cascade of gas-phase collisions in the presence of O_2 ; (d) collision-induced dissociation of O_2 yields AOs with adequate kinetic energy which can cause additional collision-induced dissociation of O_2 . Computational simulations of such collisions, with both ab initio molecular dynamics and direct simulation Monte Carlo methods, are used to guide the experimental generation of the proposed AO-beam. We experimentally demonstrate the highest known AO mean flux-density of about 1.5×10^{16} atoms $cm^{-2} s^{-1}$ in a broad-beam, and use it to oxidatively modify a self-assembled molecular layer of siloxane on a silicon wafer. In addition, we also demonstrate the growth of Al_2O_3 through an AO-assisted atomic layer deposition process at a room temperature.

KEYWORDS. Collision, Molecular dynamics, Monte Carlo, Oxidization, Atomic layer deposition

Introduction

Atomic oxygen (AO), generated by the dissociation of molecular oxygen, exhibits high chemical reactivity and has been extensively employed in investigating material oxidation and corrosion mechanisms, as well as in developing novel oxidation processes in the chemical industry.[1-6] Particularly, the generation of a broad beam of AOs for the controlled growth of a metal-oxide monolayer and the controlled oxidative-etch of an organic/carbonaceous device-constituent is highly desirable to fuel the emergency of 2-dimensional structures with a monolayer accuracy in advanced electronics, optoelectronics and other functional devices.[7-9] For example, atomic layer deposition (ALD) of metal-oxide has indeed become a crucial technique in many device-manufacturing processes but its practical exploitation has been stalled by the difficulty in quickly purging the water vapor which is used to oxidize the metal-oxide precursor.[10-13] In principle, AO is more active than water vapor and AO can be purged quickly. In the engineering design of an AO-beam generator for practical manufacturing, the flux-density of AOs should be considerably higher than 10^{15} atoms $cm^{-2} s^{-1}$ in order to support the growth/etch of a monolayer-substance per second, with a broad beam covering an area of not less than $300cm^2$. An option of pulsing the AO-beam on and off every second further enables the precise control of monolayer-wised oxide-growth and etching per second. Such an AO-beam generator is ideal but has been generally conceived to be technically infeasible.

Historically, the development of an AO broad-beam was first quested for the facilitation of space-exploration. In brief, when space-crafts and artificial satellites operate within low Earth orbit (LEO), chemical reactions causing detrimental damage of such space-facilities occur because the presence of O_2 in LEO dissociates into AO by solar ultraviolet irradiation and AO colliding with space-facilities traveling at a sonic speed is violent and reactive. More specially, the kinetic energy of such AO (about 5eV) indeed matches the molecular chemical bond strength (3-5eV) of typical materials and an AO flux of 10^{15} atoms $cm^{-2} s^{-1}$ is sufficient to cause collision-induced chemical-modification of one monolayer per second.[14] As such, the research in this specialized field has fostered the development of AO-beam equipment with controllable kinetic energy up to 5eV and high throughput (10^{15} atoms $cm^{-2} s^{-1}$). This, in turn, can facilitate the investigation of novel oxidation mechanisms and applications by regulating the kinetic energy and throughput of AOs.

However, the development of high-throughput AO-beam equipment is stalled by numerous technical limitations and difficulties.[14, 15] First, although AOs can be readily produced by pyrolysis, photodissociation and plasma-reactions, the kinetic energy of AOs thus produced is uncontrollable and typically in a tame region of a few meV. [16-20] Technically, hyperthermal AOs with kinetic energy up to 10eV can be generated by the well-established molecular-beam technology via high-pressure-jet acceleration of O_2 , with laser-dissociation of the accelerated O_2 . [20, 21] Practically, this costly method can typically give an AO-beam with a cross-sectional diameter not more than 1mm, and is thus suitable for fundamental research but not for engineering of industrial exploitations. In this context, industrial engineering has turned to the adoption of the electron-cyclotron-resonance (ECR) plasma technology which is known to facilitate the most intensive ionization-induced dissociation of molecules in gas phase, including the dissociation of O_2 into AOs and oxygen ions.[22] Oxygen ions thus generated are extracted from the plasma and then accelerated by an electric field to regulate their kinetic energy. They are finally converted to AOs with the desirable kinetic-energy by collision and charge-transfer with a metal-plate mounted near the exit of the oxygen ion beam

extracted from the ECR plasma. This technology has indeed been used to produce an AO-beam of about 5eV in kinetic energy, with a cross-sectional beam diameter of about 20cm. The AO-beam size is limited by the practical size of an ECR plasma source. This known demonstration of a practical broad AO-beam with a controllable kinetic energy has, nevertheless, the following deficiencies: (a) the AO flux density is limited by the ion flux density and even an ECR plasma can only support a maximum ion flux density of about 1×10^{15} ions $\text{cm}^{-2} \text{s}^{-1}$ and a beam of about 300cm^2 ; (b) ion neutralization by charge-transfer with a metal-plate inevitably leads to ion-sputtering and metal-contamination of the AO-beam; (c) the AO-beam must be used close to the ion-exit from the plasma in order to prevent a severe flux-density drop caused by broadening of the ion beam and AO-beam. The placement of a workpiece-specimen close to a plasma which gives strong ultraviolet radiation and excited atoms/molecules, however, risks detrimental damages of the specimen.

Here, an innovative and practical method is reported to overcome the deficiencies of this AO-beam technology. The present innovation articulates the science and technology of converting a broad ECR-based oxygen-ion beam with a flux of 1×10^{15} ions $\text{cm}^{-2} \text{s}^{-1}$ to a broad AO beam with a flux of 1.5×10^{16} atoms $\text{cm}^{-2} \text{s}^{-1}$ via collision-induced dissociation of O_2 into AOs, as shown in **Figure 1**. In this AO generator, one ion injection with a kinetic energy of 300eV initiates many collision cascades in which on the average about 130eV of the 300eV injection-energy is used to drive about 24 O_2 dissociations each costing a dissociation energy of about 5.1eV. Since ion extraction can be easily pulsed, the resultant AO flux can also be engineered with a pulsing frequency not less than one on/off cycle per second. The objective is the facilitation of industrial exploitation of AO surface-modification and AO-assisted metal-oxide deposition, to realize the rising demands of layer-by-layer surface-modification/deposition with a controlled operation of one atom/molecular monolayer per second, with a scalable modification/deposition area of $[?]1000 \text{cm}^2$. In the following sections, the fundamental concepts of AO generation by gas-phase dissociative collisions initiated by oxygen ions extracted and accelerated from an oxygen plasma are explained by ab initio molecular dynamics (AIMD) of the kinematics in dissociative O^+-O_2 , $\text{O}-\text{O}_2$ and O_2-O_2 paired-collisions, particularly to pin-point the threshold kinetic energy required for O_2 dissociation in different collision-impact trajectories. With these critical attributes, direct simulation Monte Carlo (DSMC) method of the generation of a high-flux AO-beam by extracting O^+ from a plasma into a low-pressure O_2 atmosphere are detailed. The simulations are then translated into the engineering designs of a practical AO-beam generator, as shown in **Figure 1**, with an AO flux density more than 10^{16} atoms $\text{cm}^{-2} \text{s}^{-1}$ and a beam $[?]1000 \text{cm}^2$ at the proximity of the generator exit, in a pulse-operation mode with a pulsing frequency as high as one on/off cycle per second. The generator comprises an array of 2-by-2 ECR plasma sources, with a total power of 800W. These functional features are demonstrated and validated. More specifically, the oxidative modification of a self-assembled molecular layer of alkyl silane on the surface of an oxidized silicon wafer is also explained. Further, the ALD of alumina with a fast rate of one-deposition cycle per 2 seconds is articulated. The supplementary information (SI) provides further elaboration on the details.

Simulations

2.1. AIMD simulations

Research on collision-induced O_2 dissociation can be dated back to the 60s when the dissociation of O_2 was driven by argon collisions in a shock-tube apparatus and the reduction of its optical absorption intensity was detected.[23] This seminal work confirmed that under such a macroscopic collision arrangement, the condition of near-thermal-equilibrium is satisfied and the rate constant of O_2 dissociation is governed by a simple Arrhenius equation such that the dissociation probability scales exponentially with $-5.1\text{eV}/k_{\text{B}}T$, where 5.1eV is the well-known dissociation energy of O_2 . In shock-tube experiments, T of 5000 to 18000K and $k_{\text{B}}T$ for argon rated at 0.65 to 2.35eV are practical. As such, simulations of such collision-induced dissociation are typically performed with classical or semi-classical methods.[24] However, the collision-induced O_2 dissociation in the present work is conducted with a condition far from thermal equilibrium and must be treated microscopically, with a diligent attention of each collision event in an atomic scale.

The advances in computational hardware and software now indeed support such microscopic tracks of col-

lisions and collision-induced dissociations. In brief, ab initio calculations of the electronic structures of all collision partners in each collision event by solving the Schrodinger equation as a function of the evolution-time with a time-division as short as 0.2fs are practically conducted. The snapshots of the coordinates, rotational/vibrational states and electronic structures of the collision partners are commonly referred as ab initio molecular dynamics (AIMD). In accord to the practical experimental setup, AIMD of some 200 representative collision events are performed by adopting O^+ to model the oxygen ion extracted from an ECR oxygen plasma into a cloud of O_2 . Although O_2^+ ions are also extracted, the practical operation of the experimental AO generator always injects oxygen ions at 300eV into a cloud of O_2 and a 300eV O_2^+ collides with O_2 is expected to effectively converted all injected O_2^+ into O^+ and O. Hence, AIMD with O^+ as bullets is reasonable. Some exemplary collision events tracked by AIMD are depicted in **Figures 2-3**, with more exemplars shown in **Figure S1**.

For example, the AIMD computational results for 300eV O^+ colliding O_2 along the molecular axis of O_2 (collision angle at 0°) are summarized in **Figure 2(a)**. Briefly, the closest encounter between the projectile and the O^I atom of O_2 occurs near 6fs, and prior to that the projectile is traveling with not any force influence until the weak van de Waals interactions prior to 3.5fs. At 3.5fs, the wavefunction of O^+ starts interacting with that of O_2 and charge exchange occurs, with an electron from the highest occupied states of O_2 tunneling to the lowest unoccupied state of O^+ . This process leads to a transfer of potential energy between the projectile and its colliding partner via electron tunneling, and virtually induces no change of the kinematics. Then, shortly after this, the encounter of O and O_2^+ becomes repulsive and the wavefunction of O starts mixing with that of O_2^+ , to form a transient molecular species which retains a configuration of O_3^+ in the time duration of about 5.5 – 7fs. In this duration, kinetic energy and molecular potential interchange in a rather peculiar way. Apparently, at about 6.7fs, the most stable O_3^+ species is formed and it flies with a kinetic energy of 300eV. Still, this most stable O_3^+ is repulsive in nature and quickly dissociates into $O-O^{I+}$ and O^{II} at about 7.5fs. Hence, although the collision is violent, the process ends with one AO and an O_2^+ , with no generation of any additional AO.

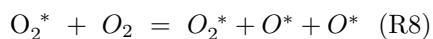
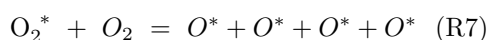
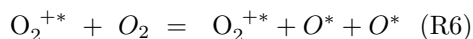
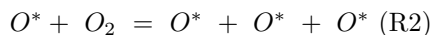
To further illustrate the collision events in an atomic scale, the isosurface evolutions of the spin density distributions of this system comprising three oxygen atoms are tracked and depicted in **Figures 2**. For example, **Figure 2(a)** shows, at 0fs, two blue isosurfaces signifying the presence of two spin-identical electrons in the px and py orbitals of the spin-polarized oxygen molecule. The spatial distributions of spin density undergo significant changes throughout the collision process.

Although the violent head-on collision with a collision angle of 0° does not yield any AO generation, a slight change in collision angle causes some surprising changes. For example, when the collision angle is changed merely by 5 degrees, the shear-like adjustment of the violent collision effectively causes the dissociation of the transient repulsive molecular species of O_3^+ into 2AOs and an O^+ . Additional AIMD calculations reveal that the production of AOs in this collision configuration of “5 degrees” can proceed as long as the incoming O^+ carries a kinetic energy more than 36eV, as shown in **Figure 2(b)**. In this case, the O^+ bullet of 36eV changes to O at about 9fs and merges with the resultant O_2^+ to form a transient O_3^+ which survives in the duration of about 12fs – 17fs. At 20fs, an AO and a highly excited O_2^+ are formed. At 25fs, the excited O_2^+ dissociates into O and O^+ . Clearly, the inset of **Figure 2(b)** illustrates that the separations among all three atomic centers are all increasing with time.

In the collision configuration when an 14eV O^+ flies head-on towards the O^I atom of O_2 with a velocity perpendicular to the O_2 molecular axis ((collision angle at 90°), a repulsive and transient O_3^+ is formed and survived for the duration of about 28fs – 50fs. But the three atomic centers slowly move away from each other and eventually dissociates into 2AOs and an O^+ . The threshold kinetic energy of the bullet O^+ for collision-induced dissociation of O_2 is 14eV for this particular collision configuration. The AIMD results are summarized in **Figure 3(a)**. By moving the flight path of O^+ merely 0.04nm away from the O^I center of O_2 , the slightly change in the collision impact parameter (therein referred as IP) causes a large increase from 14 to 54eV in the dissociation threshold in reference to the kinetic energy of the O^+ bullet, as shown in **Figure 3(b)**. A comparison of the head-on case in **Figure 3(a)** and the IP at 0.04nm case in **Figure 3(b)** validates

the intuitive expectation that the kinematic changes of O^I which is the principal collision partner hit by the O^+ bullet is less “sloppy” in the case of the head-on collision case.

In short, the AO-generation thresholds critically depend on the exact collision configurations and some representative values are summarized in **Table 1**. Consequently, this results strongly support the likelihood of the following reaction kinematics involving charge-transfer and dissociative collisions (with a label of * to denote the hyperthermal nature of a reactant):



For example, in R1, a hyperthermal O^+ with 300eV violently collides with an O_2 and this leads to the dissociation of O_2 into two hyperthermal AOs. With a sufficiently high kinetic energy, a resultant hyperthermal atomic oxygen may again cause the collision-induced dissociation of an O_2 , a reaction which yields three hyperthermal AOs. In R3, charge transfer between O^+ and O_2 is noted, together with kinetic energy transfer. Similarly, charge transfer between an O_2^{+*} and an O_2 is noted in R4, together with kinetic energy transfer. In R5, an O_2^{+*} with a sufficiently high kinetic energy causes an extremely violent collision-induced dissociation of itself and the collided O_2 , with the production of four hyperthermal AOs. In comparison, R6 depicts a less violent event with only one case of dissociation. R7 and R8 are counterparts of R5 and R6, with O_2^* replacing O_2^{+*} as the “bullet”. The present work tracks all these reactions and statistically sizes up the essences in the AO generation by injecting 300eV O^+ into a cloud of O_2 at 0.14Pa.

2.3. DSMC method

In reference to the experimental design of an AO generator illustrated in **Figure 1**, the well-known direct simulation Monte Carlo (DSMC) method is adopted to track the cascades of collisions induced by the injection of 300eV O^+ into the tube chamber of the AO generator, with an O_2 pressure of 0.14Pa in the chamber.[25-30] Briefly, the conditions of rarefied gas dynamics are assumed, the Boltzmann equation describing the dynamic behaviors of the gaseous species in a single intake of O_2 flowing through the tube chamber, with and without the injection of a 300eV O^+ are solved with the computational treatments extensively elucidated by Bird.[30]

An exemplar of a collision event simulated by this DSMC approach is depicted in **Figure 4**, with the snapshots in the right column representing the process of a pulse of O_2 flowing through the collision chamber modeled as a tube. This pulse of O_2 flowing through the collision chamber is assumed to have an average molecular density of $0.4 \times 10^{-3} M$. The exact molecular density distribution at each geometric location at a given time is random, and can be higher or lower than this average molecular density due to Brownian motions. The pumping operation moves this pulse of O_2 at a speed of about 80cm per 0.65ms. In comparison, the snapshots in the left column depicts the evolutions of collision cascades induced by the activation of the O^+ injection electrode. More specifically, the left snapshot of **Figure 4(a)** shows a blue spot (a drop in molecular density) at the middle section of the tube at the snapshot time of 0.07ms. Since in the presence of an average molecular density of $0.4 \times 10^{-3} M$ of O_2 , the average collision mean-free-path of O is about 8cm, the location of this blue spot at the middle-section of the tube (40cm from the left tube-opening) implies that the injected O^+ has gone through about 3 collisions with large impact-parameters, i.e., 3 “missing-target” collisions with little energy-loss to its collision partners. At time near 0.07ms, a head-on collision

has occurred and a cascade of collisions has been initiated. Some O_2 molecules engaging themselves in this first cascade of collisions are moving away from the central location of the cascade. This causes a drop in the molecular density and the evolution of the blue spot. In the left snapshot of **Figure 4(a)**, additional cascades of collisions have been initiated by the first cascade of collisions at the snapshot time of 0.15ms, particularly at the proximity of the first cascade of collisions but several cascades of collisions have also been randomly generated far away from the first cascade of collisions. The presence of such “follow-up” cascades of collisions all induce a drop in molecular density and can be located by those blue spots in the snapshot. While most “blue spots” are moving forward to the right exit of the tube, some “blue spots” are moving backward to the left entrance of the tube, as random backscattering is inevitable. The left snapshot of **Figure 4(c)** shows that the first aggregate of collision-cascades is exiting the tube at 0.25ms. Since this aggregate of collision-cascades leaves the tube quickly, the “bullet” initiating the collisions must carry a relatively high kinetic energy; as such, dissociation-collisions may have occurred. If so, some AOs exit the tube at 0.25ms. Similarly, the probability of AO production near the first cascade of collisions depicted by the blue spot in the left snapshot of **Figure 4(a)** is high. Hence, the left snapshot of **Figure 4(f)** predicts that a relatively high flux of AOs leaves the tube at the snapshot time of 0.55ms.

In short, coupling AIMD and DSMC simulations confirms adequate AO generation by firing 300eV O^+ into a cloud of O_2 at a 0.14Pa, and offers fundamental mechanistic understanding of the relevant dissociative and non-dissociative events in this innovation technology for generating a high flux of AOs.

Experiments for the Generation and Exploitations of AOs

Design and Operation of a Practical High-Flux-AO Generator

The AO generator depicted in **Figure 1** comprises four compact ECR heads each with a power of 200W, arranged in a close-packed array as an expandable plasma source. The mesh electrodes coupled to the O_2 plasma source allow the extraction of positively charged oxygen ions which are mainly O^+ , with a kinetic energy of 300eV into the drift-tube with a diameter of 30cm. For a total power of 800W, the experimental data in the present work show that the ion flux density can reach 1×10^{15} atoms $cm^{-2} s^{-1}$ at the extraction aperture with a beam of $300cm^2$. While the ion flux density is practically confined to this level, the diameter of the plasma source and ion source can be expanded by incorporating more compact ECR heads. Perceivably, an array of 9 ECR heads, with a total power of 1800W, can be used to make an ion source with a beam near $700cm^2$ with an ion flux density of 1×10^{15} ions $cm^{-2} s^{-1}$.

Three aperture electrodes are incorporated in the drift-tube to facilitate ion extraction into the drift tube for the production of AOs in the drift-tube and to limit ions and hot-electrons leaving the exit-end of the drift-tube for the prevention of undesirable damage of the workpiece-specimen placed at the exit of the AO generator. They are also aligned such that the ultraviolet radiation from the intense plasma is blocked.

In the operation of the AO generator, the number of non-dissociative collision partners n is determined by both the length of the drift chamber and the mean free path of O_2 :

$$n = 2^{\frac{l}{\lambda}} \quad (1)$$

$$\lambda = \frac{-\mu v_m}{P} \quad (2)$$

$$v_m = \left(\frac{2K_B T}{m} \right)^{\frac{1}{2}} \quad (3)$$

where l and λ respectively represent the length of the drift chamber and the mean free path of O_2 ; μ is gaseous viscosity; P denotes the O_2 pressure in the drift-tube; v_m represents the most probable velocity

of O_2 ; K_B is the Boltzmann constant; T is the temperature in the drift-tube, and m is the mass of O_2 . The length of the drift chamber in this work is 80cm. In a typical operation, P is 0.14 Pa, T is 300K and λ is 8cm; as such, the number of non-dissociative collisions can be roughly 1000. Among these collision partners, only one carries a positive charge in the completion of all these collisions; thus, charge transfer is not particularly important. The average energy of these particles is roughly about 175meV. Hence, they are slightly more chemically active than their counterparts at 300K. As for AO generation, merely the first 2-4 rounds of collision-cascades initiated by a 300eV O^+ are violent enough to cause O_2 dissociation. The following Kapton erosion tests reveal that on the average, 24 O_2 dissociations are induced by one 300eV oxygen ion injection.

3.2 Estimations of the AO Flux-Density generated by the AO Generator

In the present work, the well-known Kapton mass loss method for measuring AO flux densities is adopted. In addition, a self-assembled monolayer (SAM) of ethyl trimethyl siloxane (ETS) formed on an oxidized silicon wafer is exposed to the AO beam of the AO generator for testing the AO oxidative behavior. Both the changes in hydrophilicity by water contact angle measurements (WCA) and surface composition by X-ray photoelectron spectroscopy (XPS) are characterized as a function of AO exposures. The experimental details are included in SI.

Results and Discussion

The experimental results from the Kapton mass loss measurements and the WCA measurements are included in **Figure S5**. In brief, the Kapton mass loss measurements confirm that for the injection of 300eV O^+ at a flux density of 1×10^{15} ions $cm^{-2} s^{-1}$ into the tube chamber of the AO generator, a broad AO beam with a flux density of 1.5×10^{16} atoms $cm^{-2} s^{-1}$ is detected at a distance of 6cm from the exit of the tube chamber. The Kapton mass loss measurements also confirm that the AO fluxes at the specimen-placement plane of 6cm from the exit plane are uniform with a change of less than 10% within the central area of 30cm in diameter. Since the tube chamber has a diameter of 30cm, the diameter of the broad AO beam at 6cm outside the tube exit is expected to be about 36cm, due to random scattering of AOs. Thus, the AO flux density right at the tube exit is expected to be 2.2×10^{16} atoms $cm^{-2} s^{-1}$ and the AO flux is 1.53×10^{19} atoms s^{-1} . Since the ion flux density of 1×10^{15} ions $cm^{-2} s^{-1}$ is injected into the tube, with an injection diameter of 20cm, the ion flux is 3.14×10^{17} ions s^{-1} . Therefore, on the average, 48.7 AOs are generated by one 300eV O^+ and roughly about 24 collision-induced dissociations of O_2 are driven by each ion injection.

As for the exploitation of AOs, a drop in WCA of 20° is evidence with one second of the AO beam-pulse onto the C_2H_5 -SAM. The surface oxidation is also revealed with the C1s XPS spectral analysis shown in Figure 5(a). In this set of data, the sample prior to any AO exposure should have a surface composition of SiO_2 terminated by $-C_2H_5$ and should thus show a C 1s spectrum of those carbon atoms in $-C_2H_5$. The trace amounts of spectral signals of C-O, C=O and O-C-O chemical species are attributed to the practically inevitable adsorption of residual carbonaceous contaminants such as lubricating oils in the non-perfect ultrahigh vacuum environment during XPS analyses. A comparison of the spectral data with and without an AO dosage of 1.5×10^{16} atoms cm^{-2} clearly shows a significant increase of the amounts of C-O, C=O and O-C-O chemical species on the AO-exposed sample. Thus, the carbonaceous contamination merely compromises but does not mask out the detection of AO-oxidation of the $-C_2H_5$ chemical group. Nevertheless, a quantitative analysis of the degree of oxidation of the $-C_2H_5$ chemical group is impossible due to this carbonaceous contamination. The drop in WCA of 20° , however, firms up the effectiveness of AO surface oxidation of a hydrocarbon surface/film.

Atomic layer deposition (ALD) of aluminum oxide is widely used as a protective encapsulant. Typically, one cycle of such an ALD process comprises a half cycle of TMA adsorption and a subsequent half cycle of TMA oxidation. Commonly, a flux of water molecules is used to complete the half cycle of TMA oxidation within a fraction of a second, but the complete purge of the residual water molecules is slow and typically requires a duration of 10 seconds or more due to the high surface sticking efficiency of water. In the present work, the flux density of 1.5×10^{16} AOs $cm^{-2} s^{-1}$ is expected to be sufficient for the completion of TMA oxidation in

less than one second and the purge of AOs is virtually instantaneous. A trial run of ALD, with one second of TMA exposure followed by one second pulse of AOs, for 50 cycles indeed yields the deposition of about 7nm of aluminum oxide on a copper disc. The XPS data summarized in **Figure 5(b)** confirms the fast deposition of aluminum oxide at room temperature with AO-assisted ALD. The effect on the passivation of a copper disc against thermal oxidation is demonstrated by the experimental evidence summarized in **Figure S5**.

Conclusion

In the present work, AIMD simulations offer clear atomistic snapshots of collision cascades induced by hiring O^+ with a kinetic energy of 0-300eV to O_2 . Dissociative collisions of O_2 and generation of AOs are evident, and the dissociation threshold requirement of the O^+ kinetic energy can be as low as 14eV which critically depends on the exact collision configuration. Through the examination of some 200 collision configurations, a comprehensive picture of collision-induced O_2 by hyperthermal O^+ is obtained. The database is then used to facilitate DSMC simulations of AO production in the practical experimental design of a high-flux AO generator equipped with an ECR oxygen ion source powered to 800W for the extraction of an ion flux density of 1×10^{15} ions $cm^{-2}s^{-1}$ with an extraction area of about $300cm^2$, and with the ions fired into a drift tube (30cm in diameter) containing O_2 at 0.14Pa. In essence, DSMC simulations confirm each 300eV O^+ bullet initiates cascades of collisions with some of them having collision energy higher than the dissociation thresholds estimated by AIMD simulations. As such, a microscopic mechanistic portrait of AO generation is yielded. Subsequent experimental AO flux density measurements by the well-known Kapton erosion method gives a quantitative estimate of 49 AOs generated by one 300eV O^+ injection. Since the dissociation energy of O_2 is about 5.1eV, on the average, about 122eV of the kinetic energy carried by each O^+ bullet is used to drive collision-induced dissociations of 24 O_2 , with the rest of input energy raising the kinetic energy and vibrational/rotational energy of each collision partners to an average of roughly 0.18eV which is significantly higher than their average energy in thermal equilibrium at room temperature. As such, the experimental AO broad-beam with a beam-size of $1000cm^2$ and a record-high flux density of 1.5×10^{16} atoms $cm^{-2} s^{-1}$ bears an average energy of 0.18eV for each AO or an AO temperature of slightly higher than $1100^\circ C$. When a self-assembled molecular layer of ethyl trimethyl siloxane on a silicon wafer is exposed to this AO beam for one second, the water contact angle drops by 20° and XPS surface analysis also confirms the surface oxidation of the hydrocarbon. In addition, the same AO-beam has also been demonstrated to facilitate the atomic layer deposition of Al_2O_3 with a record-fast growth rate of 7nm per 100 seconds. In comparison, the typical growth with water vapor to replace AO as the oxidizing agent has a typical growth rate of 7nm per 500-1000 seconds. The present work thus articulates the science and technology of practically generating a high-flux broad-beam of AOs and demonstrates some applications of such a technology innovation.

Author Contributions

Zhiqiang Han: Investigation, Writing – original draft. **Liying Song** : Formal analysis. **Po-Wan Shum** : Methodology. **Woon-Ming Lau** : Methodology, Writing - Review & Editing, Project administration.

Conflicts of interest

The authors declare that they have no known competing financial interests or personal relationships that could have appeared to influence the work reported in this paper.

Acknowledgements

We thank the financial support from National Natural Science Foundation of China (NSFC No. 22008007) and Scientific and Technological Innovation Foundation of Shunde Graduate School, USTB (BK21BE010) Foshan Science and technology Innovation Project (No. 2018IT100363). The authors declare that they have no known competing financial interests or personal relationships that could have appeared to influence the work reported in this paper.

References

1. R. Hansen, J. Pascale, T. De Benedictis and P. Rentzepis, Effect of atomic oxygen on polymers, *J. Polym.*

Sci., Part A: Gen. Pap. , 1965, **3** , 2205-2214.

2. D. H. Parker, M. E. Bartram and B. E. Koel, Study of high coverages of atomic oxygen on the Pt (111) surface, *Surf. Sci.* , 1989,**217** , 489-510.

3. T. Engel, The interaction of molecular and atomic oxygen with Si (100) and Si (111), *Surf. Sci. Rep.* , 1993, **18** , 93-144.

4. T. S. Kim, J. Gong, R. A. Ojifinni, J. White and C. B. Mullins, Water activated by atomic oxygen on Au (111) to oxidize CO at low temperatures, *J. Am. Chem. Soc.* , 2006, **128** , 6282-6283.

5. N. A. Vinogradov, K. Schulte, M. L. Ng, A. Mikkelsen, E. Lundgren, N. Martensson and A. Preobrajenski, Impact of atomic oxygen on the structure of graphene formed on Ir (111) and Pt (111), *J. Phys. Chem. C* , 2011, **115** , 9568-9577.

6. H. Li, H. Shang, F. Jiang, X. Zhu, Q. Ruan, L. Zhang and J. Wang, Plasmonic O₂ dissociation and spillover expedite selective oxidation of primary C–H bonds, *Chem. Sci.* , 2021, **12** , 15308-15317.

7. F. Le Formal, N. Tétreault, M. Cornuz, T. Moehl, M. Grätzel and K. Sivula, Passivating surface states on water splitting hematite photoanodes with alumina overlayers, *Chem. Sci.* , 2011,**2** , 737-743.

8. R. J. Kamire, M. B. Majewski, W. L. Hoffeditz, B. T. Phelan, O. K. Farha, J. T. Hupp and M. R. Wasielewski, Photodriven hydrogen evolution by molecular catalysts using Al₂O₃-protected perylene-3,4-dicarboximide on NiO electrodes, *Chem. Sci.* , 2017, **8** , 541-549.

9. S. Chandrasekaran, N. Kaeffer, L. Cagnon, D. Aldakov, J. Fize, G. Nonglaton, F. Baleras, P. Mailley and V. Artero, A robust ALD-protected silicon-based hybrid photoelectrode for hydrogen evolution under aqueous conditions, *Chem. Sci.* , 2019, **10** , 4469-4475.

10. F. Rahman and J. C. Runyon, Atomic layer processes for material growth and etching—a review, *IEEE T.SEMICONDUCT. M.* , 2021,**34** , 500-512.

11. S. Das, A. Sebastian, E. Pop, C. J. McClellan, A. D. Franklin, T. Grasser, T. Knobloch, Y. Illarionov, A. V. Penumatcha and J. Appenzeller, Transistors based on two-dimensional materials for future integrated circuits, *Nat. Electron.* , 2021, **4** , 786-799.

12. Q. Liu, M. Ranocchiari and J. A. van Bokhoven, Catalyst overcoating engineering towards high-performance electrocatalysis, *Chem. Soc. Rev.* , 2022, **51** , 188-236.

13. X. Xu, T. Guo, H. Kim, M. K. Hota, R. S. Alsaadi, M. Lanza, X. Zhang and H. N. Alshareef, Growth of 2D materials at the wafer scale, *Adv. Mater.* , 2022, **34** , 2108258.

14. *US Pat.*, 4649273, 1987.

15. *US Pat.*, 5681535, 1997.

16. C. Lee, D. Graves, M. Lieberman and D. Hess, Global model of plasma chemistry in a high density oxygen discharge, *J. Electrochem. Soc.* , 1994, **141** , 1546.

17. M. Naddaf, V. Bhoraskar, A. Mandale, S. Sainkar and S. Bhoraskar, Characterization of atomic oxygen from an ECR plasma source, *Plasma Sources Sci. Technol.* , 2002, **11** , 361.

18. I. Korolov, D. Steuer, L. Bischoff, G. Hübner, Y. Liu, V. Schulz-Von der Gathen, M. Böke, T. Mussenbrock and J. Schulze, Atomic oxygen generation in atmospheric pressure RF plasma jets driven by tailored voltage waveforms in mixtures of He and O₂, *J. Phys. D: Appl. Phys.* , 2021, **54** , 125203.

19. D. Katsube, S. Ohno, S. Takayanagi, S. Ojima, M. Maeda, N. Origuchi, A. Ogawa, N. Ikeda, Y. Aoyagi and Y. Kabutoya, Oxidation of Anatase TiO₂ (001) Surface Using Supersonic Seeded Oxygen Molecular Beam, *Langmuir* , 2021, **37** , 12313-12317.

20. E. Grossman, I. Gouzman, V. Viel-Inguibert and M. Dinguirard, Modification of a 5-eV atomic-oxygen laser detonation source, *J. Spacecr. Rockets* , 2003, **40** , 110-113.

21. M. Tagawa, R. Okura, W. Ide, S. Horimoto, K. Ezaki, A. Fujita, K. Shoda and K. Yokota, Laser-detonation hyperthermal beam source applicable to VLEO environmental simulations, *CEAS Space Journal* , 2021, DOI: 10.1007/s12567-021-00399-9, 1-9.

22. S. Duo, M. Li, Y. Zhang and Y. Zhou, A simulator for producing of high flux atomic oxygen beam by using ECR plasma source, *J. Mater. Sci. Technol.* , 2004, **20** , 759-762.

23. K. L. Wray, Shock-Tube Study of the Coupling of the O₂-Ar Rates of Dissociation and Vibrational Relaxation, *J. Chem. Phys.* , 1962,**37** , 1254-1263.

24. K. Koura, A set of model cross sections for the Monte Carlo simulation of rarefied real gases: Atom-diatom collisions, *Phys. Fluids* , 1994, **6** , 3473-3486.

25. W. Wagner, A convergence proof for Bird’s direct simulation Monte Carlo method for the Boltzmann equation, *J. Stat. Phys.* , 1992,**66** , 1011-1044.

26. B. L. Haas, D. B. Hash, G. A. Bird, F. E. Lumpkin III and H. A. Hassan, Rates of thermal relaxation in direct simulation Monte Carlo methods, *Phys. Fluids* , 1994, **6** , 2191-2201.

27. M. Gad-el-Hak, The fluid mechanics of microdevices—the Freeman scholar lecture, *J. Fluids Eng.* , 1999, **121** , 29.

28. A. A. Alexeenko, S. F. Gimelshein and D. A. Levin, Reconsideration of low Reynolds number flow-through constriction microchannels using the DSMC method, *J. Microelectromech. Syst.* , 2005, **14** , 847-856.

29. A. J. Lofthouse, L. C. Scalabrin and I. D. Boyd, Velocity slip and temperature jump in hypersonic aerothermodynamics, *J. Thermophys. Heat Transfer* , 2008, **22** , 38-49.

30. G. Bird, Comment on “Direct simulation Monte Carlo method for an arbitrary intermolecular potential” [Phys. Fluids 24, 011703 (2012)], *Phys. Fluids* , 2013, **25** .

31. R. LMNO Engineering, and Software, Ltd, Gas Viscosity Calculator, <https://www.lmnoeng.com/Flow/GasViscosity.php>).

Table 1. The threshold kinetic energy required for O₂ dissociation in different collision-impact trajectories. The symbol “[?]” denotes that the direction of the “bullet” is perpendicular to the O₂ molecular axis and hitting the middle of the O₂ bond. The symbols “[?]” and “+” special cases denote an O₂ “bullet” flying towards a target O₂ with their center-of-mass aligned and respectively with their molecular axes parallel and perpendicular to each other. The unit is eV.

collision-impact trajectories	0°	5°	60°	90°	IP=0.04nm	”[?]”	”[?]”	”+”
O ⁺ -O ₂	>300	36	33	14	54	40		
O-O ₂	>300	24	27	12	16	28		
O ₂ -O ₂	>300		>300	>300		8	>300	8

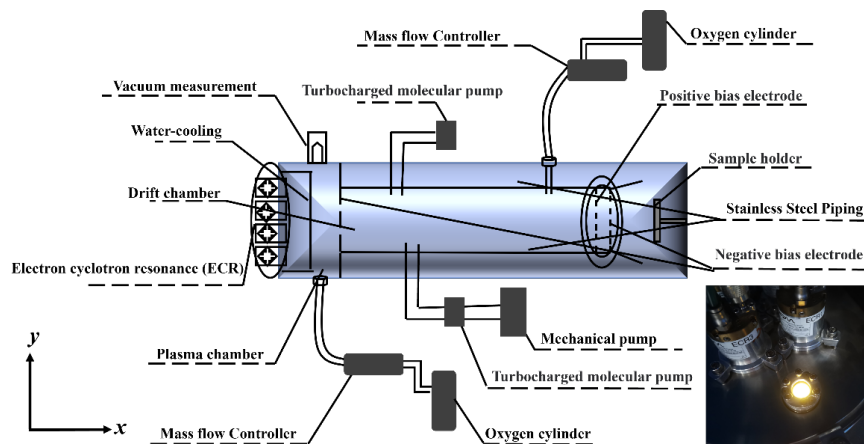


Figure 1. Schematic diagram of the broad and high-flux AO-beam generator.

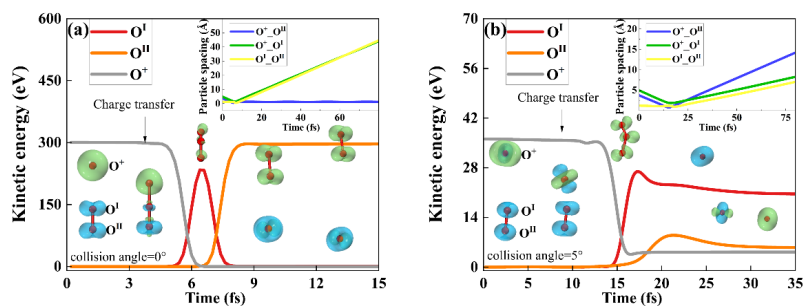


Figure 2. (a) 300eV O^+ colliding with O_2 with O^+ traveling at 0 degrees in reference to the molecular axis of O_2 and hitting head-on O^I of O_2 , no dissociation at 300eV; (b) 36eV O^+ traveling at 5 degrees in reference to the molecular axis of O_2 and hitting head-on O^I of O_2 , dissociation evident at 36eV.

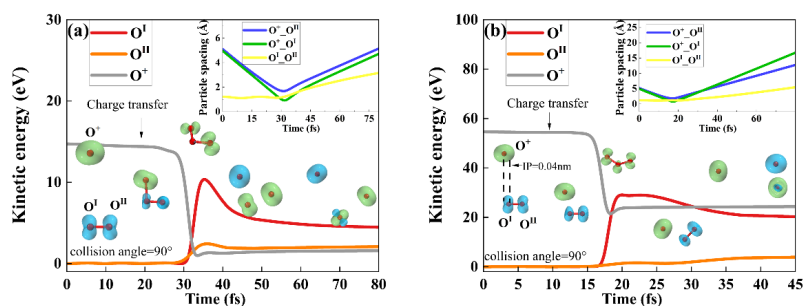


Figure 3 (a) 14eV O^+ colliding with O_2 : with O^+ traveling at 90 degrees in reference to the molecular axis of O_2 and hitting head-on O^I of O_2 , dissociation evident at 14eV; (b) 54eV O^+ traveling at 90 degrees in reference to the molecular axis of O_2 and hitting O^I of O_2 by missing the head-on condition by 0.04nm, dissociation evident at 54eV and no dissociation for collision energy less than 54eV.

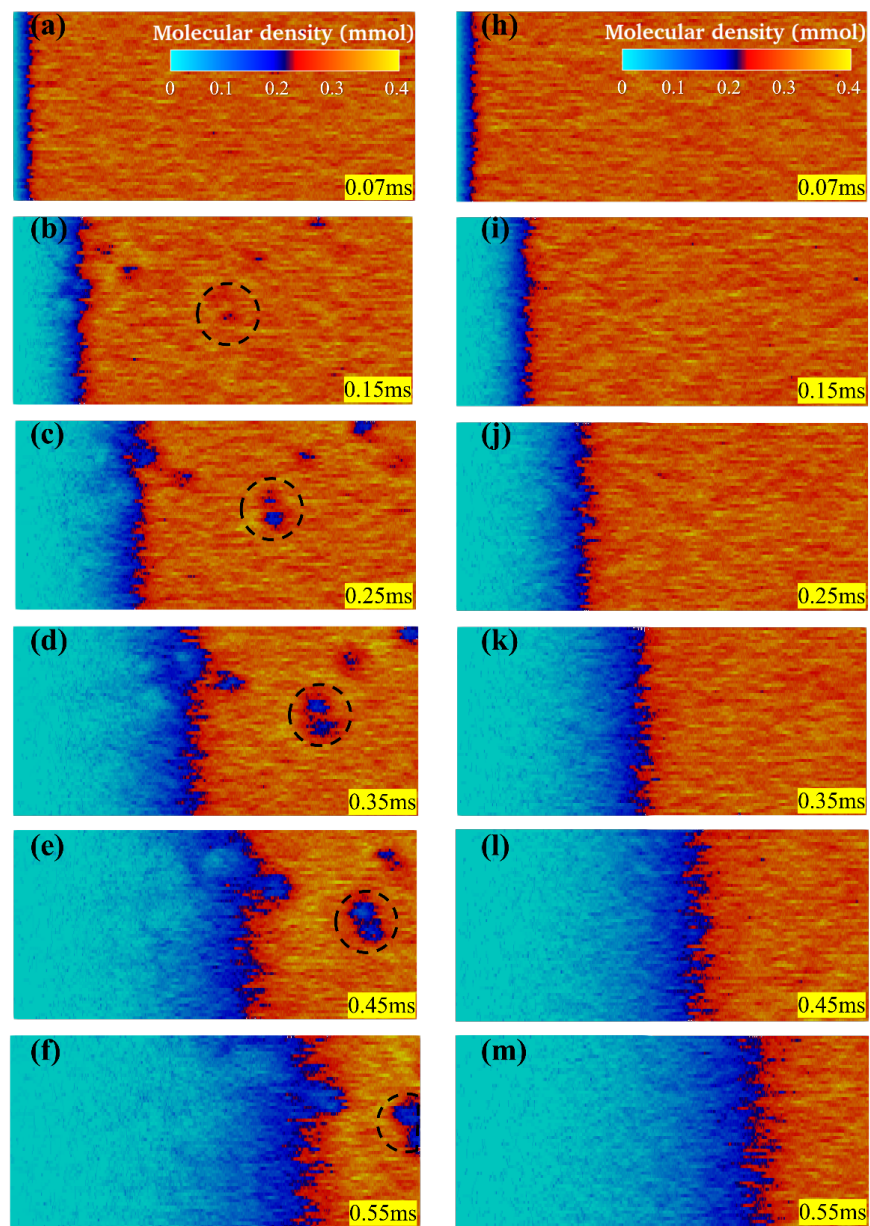


Figure 4. DSMC simulation results of O_2 distributions in a drift-tube chamber at 300K. (a)-(f) represent the activation of the -300V aperture electrode for the injection of O^+ at 300eV, while (h)-(m) represent the deactivation of the electrode and the absence of collision-cascades induced by the injection of 300eV O^+ .

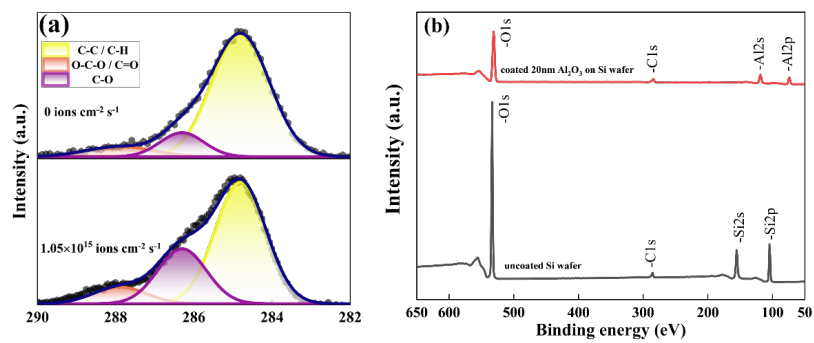


Figure 5. (a) C1s high resolution XPS results of ETS/silicon with and without the AO exposure dosage of 1.5×10^{16} AOs cm^{-2} ; (b) XPS survey spectra of an uncoated Si wafer and of 7nm Al_2O_3 formed by AO-assisted ALD on a Si wafer.